Article

Immunity

Structural Analysis Reveals that Toll-like Receptor 7 Is a Dual Receptor for Guanosine and Single-Stranded RNA

Graphical Abstract

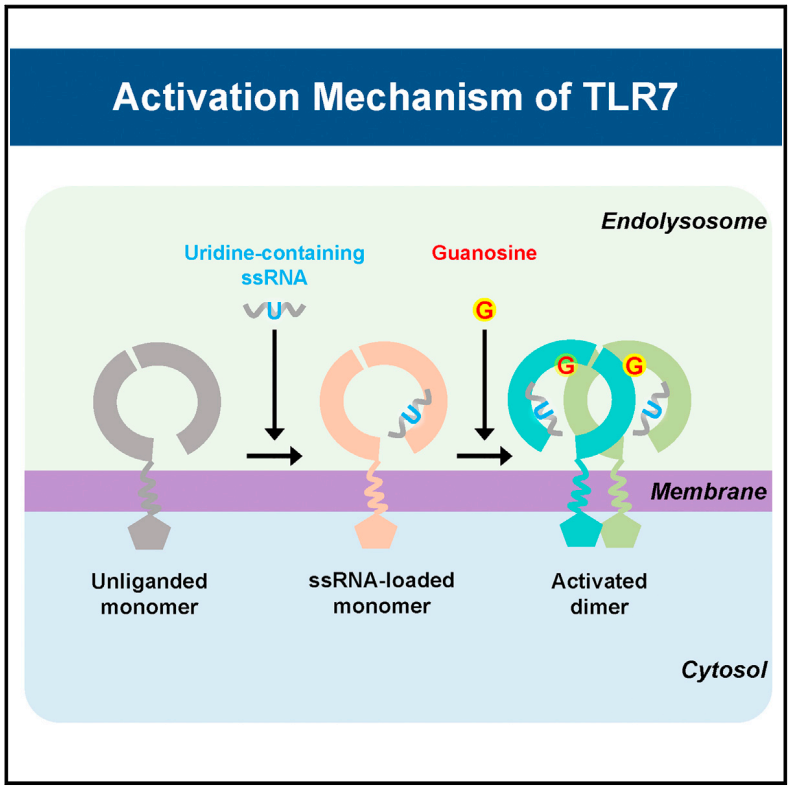

Authors

Zhikuan Zhang, Umeharu Ohto, Takuma Shibata, ..., Susumu Uchiyama, Kensuke Miyake, Toshiyuki Shimizu

Correspondence

shimizu@mol.f.u-tokyo.ac.jp

In Brief

TLR7 is a ssRNA sensor that also responds to guanosine and chemical ligands, but how these ligands activate TLR7 remains largely unknown. Zhang et al. determined the tertiary structure of TLR7 in its activated form induced by guanosine and ssRNA and reveal the ligand specificity and activation mechanism of TLR7.

Highlights

- Determined three crystal structures of activated forms of TLR7
- TLR7 harbors two binding sites, first site for small ligands and second site for ssRNA
- TLR7 is a dual sensor for guanosine and uridine-containing ssRNA
- TLR7 is synergistically activated by guanosine and ssRNA

Accession Numbers

5GMF
5GMG
5GMH

Zhang et al., 2016, Immunity *45*, 737–748
October 18, 2016
http://dx.doi.org/10.1016/j.immuni.2016.09.011

CellPress

CellPress

Structural Analysis Reveals that Toll-like Receptor 7 Is a Dual Receptor for Guanosine and Single-Stranded RNA

Zhikuan Zhang,[1,6] Umeharu Ohto,[1,6] Takuma Shibata,[2] Elena Krayukhina,[3] Masato Taoka,[4] Yoshio Yamauchi,[4] Hiromi Tanji,[1] Toshiaki Isobe,[4] Susumu Uchiyama,[3,5] Kensuke Miyake,[2] and Toshiyuki Shimizu[1,7,*]
[1]Graduate School of Pharmaceutical Sciences, The University of Tokyo, 7-3-1 Hongo, Bunkyo-ku, Tokyo 113-0033, Japan
[2]Division of Innate Immunity, Department of Microbiology and Immunology, The Institute of Medical Science, The University of Tokyo, 4-6-1 Shirokanedai, Minato-ku, Tokyo 108-8639, Japan
[3]Graduate School of Engineering, Osaka University, 2-1 Yamadaoka, Suita 565-0871, Japan
[4]Department of Chemistry, Graduate School of Science and Technology, Tokyo Metropolitan University, Minami-osawa 1-1, Hachioji, Tokyo 192-0397, Japan
[5]Okazaki Institute for Integrative Bioscience, National Institutes of Natural Sciences, 5-1 Higashiyama, Myodaiji, Okazaki, Aichi 444-8787, Japan
[6]Co-first author
[7]Lead Contact
*Correspondence: shimizu@mol.f.u-tokyo.ac.jp
http://dx.doi.org/10.1016/j.immuni.2016.09.011

SUMMARY

Toll-like receptor 7 (TLR7) is a single-stranded RNA (ssRNA) sensor in innate immunity and also responds to guanosine and chemical ligands, such as imidazoquinoline compounds. However, TLR7 activation mechanism by these ligands remain largely unknown. Here, we generated crystal structures of three TLR7 complexes, and found that all formed an activated m-shaped dimer with two ligand-binding sites. The first site conserved in TLR7 and TLR8 was used for small ligand-binding essential for its activation. The second site spatially distinct from that of TLR8 was used for a ssRNA-binding that enhanced the affinity of the first-site ligands. The first site preferentially recognized guanosine and the second site specifically bound to uridine moieties in ssRNA. Our structural, biochemical, and mutagenesis studies indicated that TLR7 is a dual receptor for guanosine and uridine-containing ssRNA. Our findings have important implications for understanding of TLR7 function, as well as for therapeutic manipulation of TLR7 activation.

INTRODUCTION

Toll-like receptors (TLRs) are membrane receptors that play a crucial role in the innate immune system (Takeuchi and Akira, 2010). TLRs are type I membrane glycoproteins that have been structurally characterized to harbor extracellular leucine-rich repeat (LRR) domain, a single transmembrane domain, and a cytoplasmic Toll/interleukin-1 receptor (TIR) domain (Bell et al., 2003; Matsushima et al., 2007). TLRs function as sensors for a limited number of pathogen-associated molecular patterns and for danger-associated molecular patterns (Aderem and Ulevitch, 2000; Janeway and Medzhitov, 2002; Takeuchi and Akira, 2010). Once TLRs recognize certain molecules through their LRR domains, such as double-stranded RNA in the case of TLR3 (Alexopoulou et al., 2001; Liu et al., 2008), lipopolysaccharide for the TLR4-MD-2 complex (Hoshino et al., 1999; Nagai et al., 2002; Ohto et al., 2012; Park et al., 2009; Poltorak et al., 1998), single-stranded RNA (ssRNA) for TLR7, TLR8, and TLR13 (Diebold et al., 2004; Heil et al., 2004; Oldenburg et al., 2012; Song et al., 2015; Tanji et al., 2013; Tanji et al., 2015), and CpG-containing DNA for TLR9 (Hemmi et al., 2000; Ohto et al., 2015), the cytoplasmic TIR domains recruit downstream TIR domain-containing adaptor molecules such as myeloid differentiation factor 88 (MyD88) and TIR domain-containing adaptor inducing interferon-β (TRIF) (Song and Lee, 2012). The signal-transduction pathways thus initiated eventually lead to the production of proinflammatory cytokines and type I interferons that mobilize host immune responses (Takeuchi and Akira, 2010).

TLRs are located either in the cell membrane or the endosomal membrane (Takeuchi and Akira, 2010). Endosome-localized TLR7 and TLR8, the TLRs that are most similar in both sequence and function, recognize viral ssRNAs, a class of imidazoquinoline compounds, and guanosine analogs (Diebold et al., 2004; Heil et al., 2003; Heil et al., 2004; Hemmi et al., 2002; Jurk et al., 2002; Lee et al., 2003; Shibata et al., 2015). Exogenous ssRNAs originating from viruses such as human immunodeficiency virus type 1 (Heil et al., 2004), hepatitis C virus (Takahashi et al., 2010), and influenza A virus (Wang et al., 2008) are considered naturally occurring ligands for these receptors, although synthetic small interfering RNAs (siRNAs) also activate TLR7 through either one or both of the separated strands (Hornung et al., 2005). Moreover, self ssRNAs such as microRNA let-7 (a gene-expression regulator in the CNS) and ssRNAs released from disrupted cells can also activate TLR7 and are regarded as causes for, respectively, neurodegeneration and autoimmune diseases such as systemic lupus erythematosus

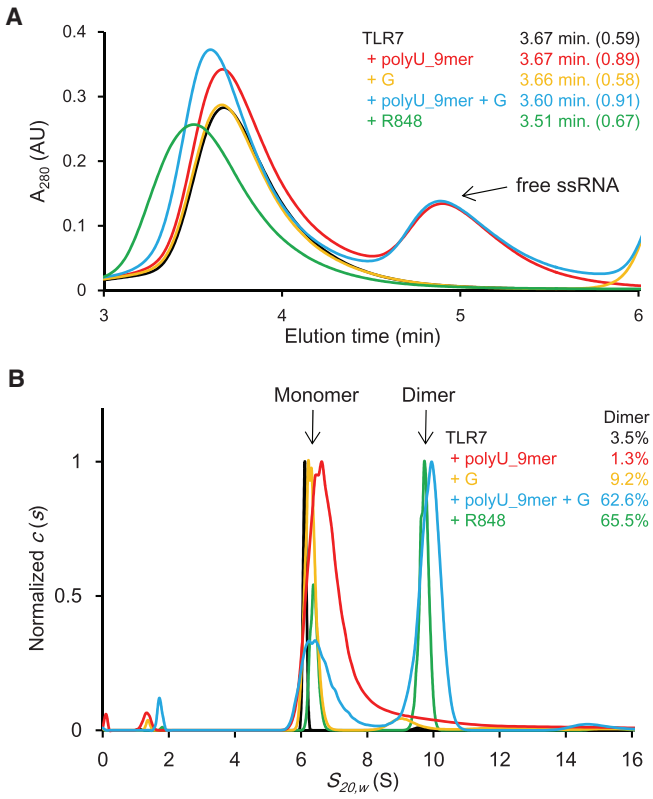

Figure 1. Agonist Ligands Induce TLR7 Dimerization

The effects of ligands on the dimerization state of TLR7 were examined using (A) gel-filtration chromatography and (B) SV-AUC analyses. TLR7 alone (black), TLR7 with polyU_9-mer (red), TLR7 with guanosine (orange), TLR7 with polyU_9-mer and guanosine (blue), and TLR7 together with R848 (green) were analyzed. The figure lists the elution times and the ratios of the absorbance at 260 and 280 nm (in parenthesis). The obtained c(s) distributions were normalized relative to the maximal value. Dimer ratios are indicated in percentages.

See also Figure S7.

(Lehmann et al., 2012; Santiago-Raber et al., 2009; Savarese et al., 2006).

Our recent studies revealed that TLR8 recognizes the degradation products of ssRNAs, uridine and short oligonucleotides, at two distinct ligand-binding sites (Tanji et al., 2013; Tanji et al., 2015), and that these two ligands synergistically activate TLR8. Furthermore, we also biochemically demonstrated that TLR7 responds to guanosine and its derivatives (Shibata et al., 2015). However, the underlying reason and mechanism of TLR7 activation by ssRNAs and small chemical ligands remain largely unknown. Specifically, why the closely related receptors TLR7 and TLR8 exhibit distinct ligand preferences is unclear. Here, we reported three crystal structures of TLR7 bound to agonist(s) and performed a biochemical and biophysical characterization of TLR7. TLR7 recognized, at distinct sites, guanosine and uridine-containing ssRNA. Synergistic coorperation of guanosine and ssRNA was required for TLR7 activation. Our results provided insights into the mechanism by which TLR7 was activated by both natural and artificial ligands, and our findings should facilitate progress in the development of therapeutic methods to target TLR7.

RESULTS

Preparation, and Biochemical and Structural Characterization of TLR7

To gain structural insight into activation mechanism of TLR7, we recombinantly expressed the extracellular domain of TLR7 from various species in *Drosophila* S2 cells. Our screening showed that among the expressed proteins, recombinant TLR7 from monkey (*Macaca mulatta*; *Mm*) (96.8% sequence identify with human TLR7) was obtained in sufficient quantities for crystallographic studies. Because the activation of TLR7-family receptors, TLR7–TLR9, requires proteolytic cleavage at the loop region between LRR14 and LRR15 (Z-loop) (Figure S1) (Ewald et al., 2011; Ewald et al., 2008; Hipp et al., 2013; Ishii et al., 2014; Park et al., 2008; Sepulveda et al., 2009), we prepared an artificially cleaved form of TLR7 by introducing a thrombin-recognition sequence before the Z-loop. All the results presented herein were obtained using the Z-loop-cleaved form of *Mm*TLR7.

First, we investigated how ligands affected the dimerization state of TLR7. Because TLR7 responds to guanosine applied in combination with polyuridine ssRNA (polyU) (Shibata et al., 2015), we used guanosine and polyU as ligands, and we also used the known agonistic chemical ligand R848. Unlike TLR8, which exists as a dimer irrespective of the presence of ligands (Tanji et al., 2013), TLR7 existed as a monomer in the absence of ligands, and TLR7 dimerization was induced by R848 alone, but not by polyU or guanosine alone, although these two ligands synergistically triggered TLR7 dimerization, as shown by the results of gel-filtration chromatography and sedimentation velocity-analytical ultracentrifugation (SV-AUC) analyses (Figure 1). Next, we screened the conditions required for crystallization and successfully obtained crystals of *Mm*TLR7 in complex with (1) guanosine and polyU_19-mer (*Mm*TLR7-G-polyU), (2) loxoribine (7-allyl-7,8-dihydro-8-oxo-guanosine) and polyU_19-mer (*Mm*TLR7-Loxo-polyU), and (3) R848 (*Mm*TLR7-R848), and then determined the structures of these three complexes (Table 1 and S1). TLR7 contained 26 LRR units with the Z-loop (residues 445–493) inserted between LRR14 and LRR15, and the TLR7 protomer formed a donut-like ring with its C- and N-termini interacting directly with each other (Figures 2A and 2B). The structures of all agonist-bound TLR7 complexes were almost identical and formed a symmetrical m-shaped homodimer in which the two C-termini of the protomers were positioned in the center, as in the case of TLR8 and TLR9 (Ohto et al., 2015; Tanji et al., 2013; Tanji et al., 2015) (Figures 2C and 2D and S2A).

Strcutural and biochemical studies showed that unliganded TLR7 was monomeric and ligand binding induced an activated m-shaped dimer of TLR7.

TLR7 Contains Two Distinct Ligand-Binding Sites for Small Ligands and ssRNA

In the *Mm*TLR7-G-polyU structure, as in the TLR8 structure, electron densities corresponding to guanosine and a portion of polyU (UUU) were observed at two distinct sites, the first and second sites, respectively (Figures 2A, 2C, 3, and S2B and S2C). The first site corresponded to the same position that was previously identified for uridine or chemical ligands in TLR8 (Tanji et al., 2015). The second site was a ssRNA-binding site, but this

Table 1. Data Collection and Refinement Statistics

	*Mm*TLR7-G-polyU	*Mm*TLR7-Loxo-polyU	*MmTLR7*-R848
Data collection			
Beamline	PF-AR NE3A	SPring-8 BL41XU	PF-AR NE3A
Space group	*P*1	$P2_1$	$P2_12_12_1$
Cell dimensions			
a, *b*, *c* (Å)	98.1, 111.3, 113.4	98.3, 99.4, 112.1	99.1, 140.1, 151.1
α, β, γ (°)	93.8, 94.3, 91.5	98.6	-
Resolution (Å)	2.50 (2.64-2.50)	2.60 (2.64-2.60)	2.20 (2.24-2.20)
R_{sym}	0.112 (0.921)	0.080 (0.410)	0.103 (0.937)
$I/\sigma I$	8.9 (1.4)	15.1 (1.8)	21.3 (1.9)
Completeness (%)	97.6 (96.3)	93.9 (88.5)	98.8 (98.1)
Redundancy	3.5 (3.6)	2.8 (2.7)	13.5 (13.1)
Refinement			
Resolution (Å)	50.0–2.50	50.0–2.59	50.0–2.20
No. reflections	153,109	58,705	100,054
R_{work} / R_{free}	0.207 / 0.243	0.215 / 0.258	0.185 / 0.224
No. atoms			
Protein	25,188	12,330	12,528
First site ligand	80	48	46
Second site ligand	256	128	-
Water	157	33	653
B-factors (Å^2)			
Protein	51.9	68.4	42.0
First site ligand	36.5	70.7	37.3
Second site ligand	62.6	69.6	-
Water	37.3	49.0	40.6
R.m.s deviations			
Bond lengths (Å)	0.013	0.012	0.017
Bond angles (°)	1.78	1.67	1.86

Each dataset was collected with one crystal. Highest resolution shell is shown in parenthesis. See also Table S1.

site of TLR7 is spatially and structurally distinct from that of TLR8: UUU in the second site of TLR7 neighbored the dimerization interface (Figures 3 and S3), whereas UG in the second site of TLR8 is completely outside the dimerization interface (Figure S4A). We performed a sequence alignment of TLR7 from multiple species and human TLR8 and found that the residues forming the first and second sites were highly conserved among TLR7 from various species (Figure S1). Moreover, between TLR7 and TLR8, the residues forming the first site were highly homologous, but the amino acid composition and location of the second site were completely different (Figures S1 and S4). The position of ssRNA in the TLR7 dimer partially overlapped with that of CpG-DNA in the TLR9 dimer (Figure S4B). In a similar manner, we modeled loxoribine and UUU into the first and second sites, respectively, in the *Mm*TLR7-Loxo-polyU structure (Figures S2A–S2C). To determine whether these structures contained UUU or a longer nucleotide with its terminal(s) disordered in the structures, we conducted liquid chromatography–mass spectrometry (LC-MS) analysis on dissolved crystals of *Mm*TLR7-G-polyU (Figure S2D). We detected guanosine and 3-mer to 5-mer polyU but only a trace amount of intact polyU_19-mer. The most abundant oligonucleotides were polyU_4mers, including pUUUU, UUUUp, and UUUU-OH. On the basis of the results of LC-MS and structural analyses, we concluded that the ssRNAs bound at the second site were a mixture of truncated polyU of distinct lengths and that the 3-mer was the smallest oligonucleotide recognized by TLR7. These results indicated that TLR7 used two distinct ligand-binding sites to detect viral ssRNAs present in the form of their degradation products.

In contrast to the aforementioned complexes, *Mm*TLR7-R848 formed an activated dimer when only the first site was occupied by R848 and the second site was empty and showed no detectable electron density (Figure 2D). This result demonstrated that chemical ligands could activate TLR7 by binding to only the first site.

Ligand Recognition at the First Site

Our results showed that all ligands at the first site were embedded in the TLR7 dimerization interface (Figures S3A and S3B) and bridged two TLR7 molecules (TLR7 and TLR7*) (Figures 3B and 4). Throughout this paper, asterisks are used to indicate the second TLR7 and its residues in dimeric TLR7. LRR8, LRR11–14, and LRR16*–18* (and LRR8*, LRR11*–14*, and LRR16–18) formed the first site (Figures 2A and S1).

In the *Mm*TLR7-G-polyU structure (Figures 3B and 4A), guanosine bound to TLR7 in the *syn* conformation, where the 5′-OH group of a ribose formed an intramolecular hydrogen bond with the N3 of a guanine base. The guanine moiety was surrounded by Y356, F408, K432, T532*, D555*, L557*, and I585*, and the ribose part of guanosine was surrounded by Y264, F351, Q354, V355, V381, L557*, I585*, and T586*. The guanine ring was sandwiched by the side chains of F408 and L557*, forming a face-to-face π-π stacking interaction with F408. Moreover, the imidazole ring of guanine engaged in a perpendicular edge-to-face NH-π interaction with the Y356 side chain. Hydrogen bonding occurred between the N1 and N2 atoms of guanine and the D555* side chain and between the carbonyl group of guanine and the K432 side chain. In contrast to the strict recognition of the guanine moiety, the ribose moiety was loosely recognized by TLR7, with one hydrogen bond formed between the 5′-OH group and the N of T586*. In the *Mm*TLR7-Loxo-polyU complex, loxoribine was recognized by TLR7 and intramolecular hydrogen bonds were formed in similar manner as in the case of guanosine (Figures 4A and 4B). The Y356 side chain was shifted by ~1 Å to accommodate the allyl group at N7 and the carbonyl group at C8 of loxoribine (Figure 4A). While several residues at the pocket entrance are distinct, the recognition mode of guanosine by TLR7 is smilar to that of uridine by TLR8 (Figure S4D).

The imidazoquinoline ligand R848 was recognized by TLR7 in manner that was both similar to and distinct from the manner in which guanosine was recognized (Figures 4A and 4C). The recognition of the quinoline moiety of R848 resembled that of the guanine base, with interactions occurring with F408 and Y356, and with L557*, and the amidine group (N1 and N2 atoms)

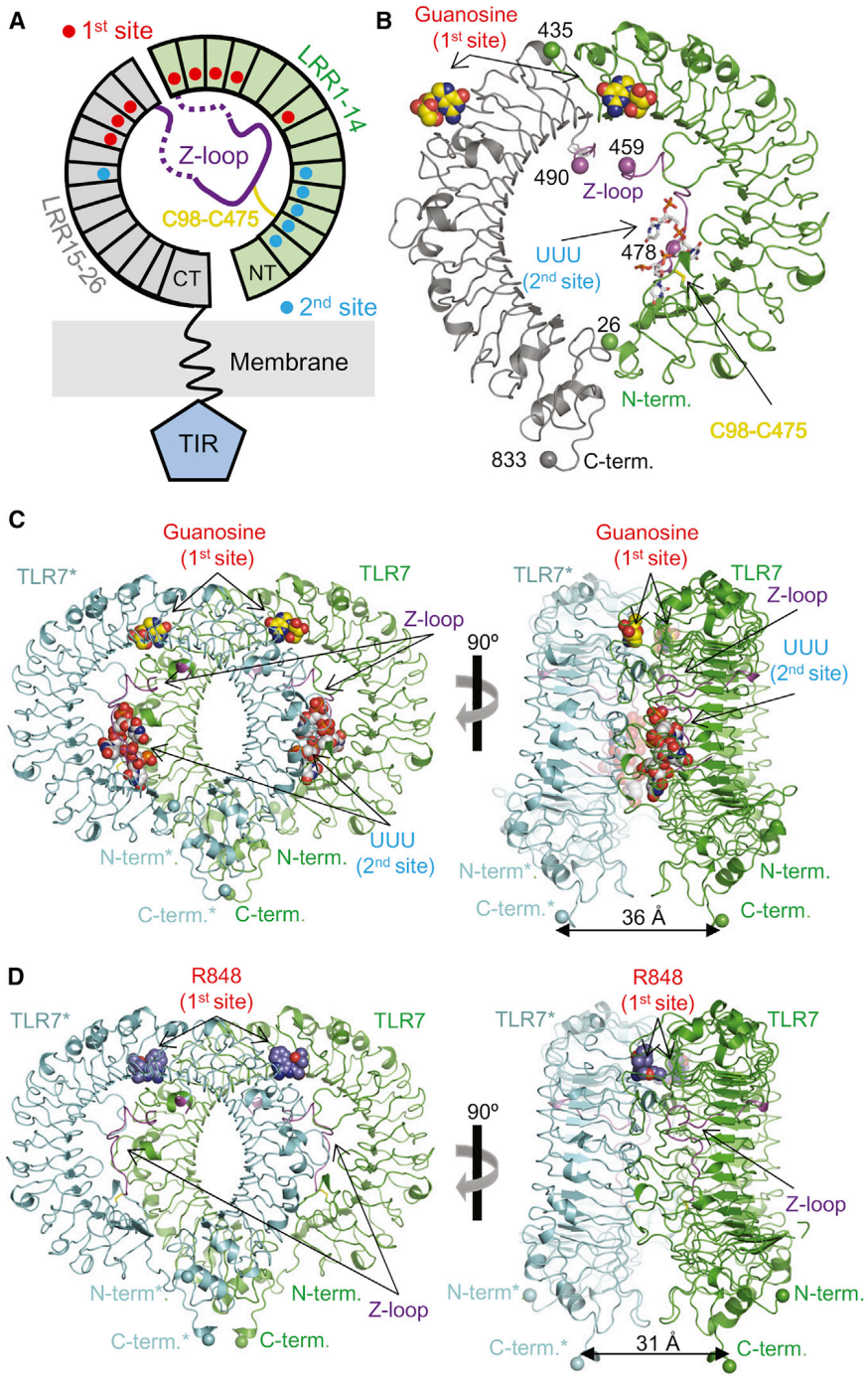

Figure 2. Agonist-Bound TLR7 Complexes Form Symmetrical M-Shaped Dimers

(A) Schematic representation of the domain organization of monkey TLR7 (*Mm*TLR7). The ring shape, the helix, and the pentagon indicate the extracellular LRR domain, the transmembrane domain, and the intracellular TIR domain, respectively. The N-terminal half (LRRNT-14), the Z-loop, and the C-terminal half (LRR15-CT) are shown in green, magenta, and gray, respectively. The LRRs that form the first site and the second site are highlighted using red and blue dots, respectively. The yellow line indicates the disulfide bond between C98 and C475.

(B) Front view of the protomer structure of the *Mm*TLR7-G-polyU dimer. Guanosine in the first site and UUU in the second site are shown in space-filling and stick representations, respectively. The N- and C-termini of each fragment are shown as spheres. The C, O, N, and P atoms of the ligands are colored yellow (guanosine) or gray (UUU), red, blue, and orange, respectively. The C98-C475 disulfide bond is shown as a yellow stick.

(C) Front (left) and side (right) views of the *Mm*TLR7-G-polyU dimer. TLR7 and its dimerization partner are colored green and cyan, respectively. The distance between the two C-termini is shown. Guanosine and UUU are recognized at the first and second sites, respectively.

(D) Front (left) and side (right) views of the *Mm*TLR7-R848 dimer shown similarly as in Figure 2C. The C atoms of R848 are colored light purple.

See also Figures S2A, S3A, and S4A–S4C.

engaged in hydrogen bonding with the D555* side chain. Conversely, additional hydrogen bonding and hydrophobic interactions were only observed in the *Mm*TLR7-R848 structure: The amidine N2 atom and the N atom of the imidazole moiety formed hydrogen bonds with T586* O and T586* N, respectively, and the ethoxymethyl group, which is a characteristic feature of R848, engaged in hydrophobic interactions with the hydrophobic pocket formed by the side chains of the residues F349, F351, V381, and F408. Furthermore, the O atom of the ethoxymethyl group interacted with G584* O through a water molecule.

In addition to ligand-protein interactions, protein-protein interactions were observed at the first site, which further contributed to TLR7 dimerization. In the *Mm*TLR7-G-polyU structure, the K432 side chain formed a salt bridge to the D555* side chain and also formed a hydrogen bond with S530* (Figure 3B). T586* formed hydrogen bonds with the side chains of Y264 and N265, and the side chains of F408, Y579*, and I585* engaged in hydrophobic interactions at the bottom of the ligand-binding pocket. Similar protein-protein interactions were also observed in the *Mm*TLR7-Loxo-polyU and *Mm*TLR7-R848 structures (Figures 4B and 4C), except that the K432 side chain was not involved in the interaction in the *Mm*TLR7-R848 structure.

Multiple interactions observed between TLR7 and the ligands defined the ligand specificity of TLR7 at the first site. In addition, ligand-mediated protein-protein interactions were also structurally important for dimerization.

ssRNA Recognition at the Second Site

In the *Mm*TLR7-G-polyU structure, UUU was encompassed by the concave surface of LRR1–5, LRR20*, and a part of the

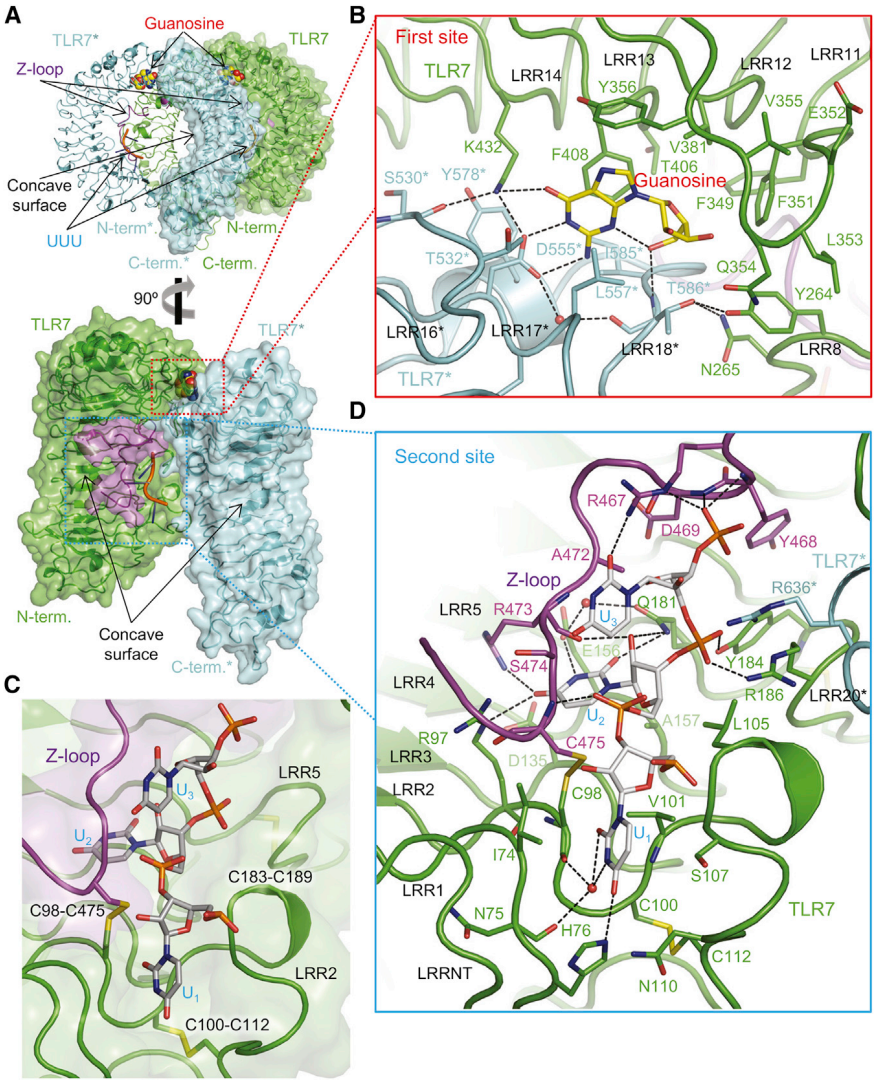

Figure 3. Guanosine and polyU Are Specifically Recognized at Two Distinct Ligand-Binding Sites

(A) Front view of the *Mm*TLR7-G-polyU dimer (top) and side view showing the concave surface of the dimer (bottom). The N-terminal and the C-terminal halves of TLR7 and TLR7*, respectively, are shown in semitransparent surface representations. UUU here is shown as a cartoon model.

(B) Detailed views of ligand recognition at the first site. The first site is composed of residues of LRR8, LRR11–14, and LRR16*–18*. Hydrogen bonds are shown as dashed lines.

(C) Disulfide bonds critical for forming the second site. The disulfide bonds C98-C475 (LRR2 and Z-loop), C100-C112 (LRR2 loop), and C183-C189 (LRR5 loop) are shown. UUU is shown in stick representation.

(D) Detailed views of UUU recognition at the second site. The second site consists of residues of the Z-loop, LRR1–5, and LRR20*. Red spheres indicate water molecules. Hydrogen bonds are shown as dashed lines.

See also Figures S2B–S2D and S3B.

Z-loop (Figures 3A, 3C, 3D and S1). The ordered region of the Z-loop of TLR7 was important for forming the second site. The structures of the Z-loop after processing differed completely among TLR7, TLR8, and TLR9 (Figure S4C). The Z-loop of TLR9 is positioned at the concave surface of the C-terminal fragment and is not associated with ligand recognition (Ohto et al., 2015). The ordered regions of the Z-loops appeared to overlap in the concave surface of the N-terminal fragment between protomers of TLR7 and TLR8, and both regions were involved in ssRNA recognition, but they were oriented in the reverse direction (Tanji et al., 2013; Tanji et al., 2015).

Disulfide bonds (C98-C475, C100-C112, and C183-C189) were also structurally important for forming the second site (Figure 3C). C475 from the latter half of the Z-loop formed a disulfide bond with C98 of LRR2 and thereby tethered the long flexible Z-loop to the concave surface of LRR by covalently linking the cleaved N- and C-terminals (Figures 2A and 2B and S4C). The C98-C475 disulfide bond was a unique feature of TLR7 (Figure S1) and is essential for the function of TLR7 (Kanno et al., 2013). Furthermore, the C100-C112 and C183-C189 disulfide bonds stabilized, respectively, the loop conformations of LRR2 and LRR5 that were directly involved in oligonucleotide recognition (Figure 3C). The structurally ordered region of the Z-loop interacted hydrophobically with LRR8 and LRR11, which formed a part of the first site. Moreover, the Z-loop and the loop regions of LRR2 and LRR5 directly participated in dimerization by interacting with LRR18*–22* (Figure S3C).

The middle U (U_2) in UUU was most strictly recognized through both uracil-specific and ribose-specific interactions (Figures 3C and 3D). The uracil base of U_2 as plunged into the pocket formed between the concave surface of the N-terminal fragment (R97, C98, D135, E156, A157, and Q181) and the Z-loop (R473, S474, and C475) and engaged in uracil-specific hydrogen bonding: the C4 carbonyl group with the side chains of R97 and R473, N3 with the E156 side chain, and the C2 carbonyl group with the Q181 side chain. The ribose-specific 2′-OH group formed hydrogen bonds with the Q181 side chain and R473 O. Both the 3′- and 5′-phosphate groups of U_2 formed hydrogen bonds with TLR7, the 3′-phosphate group with the side chains of Y184 and R186, the 5′-phosphate group with the N of C475. In contrast to the completely buried U_2 base, U_1 and U_3 bases were partially exposed to the solvent and only two base-mediated hydrogen bonds were observed, between the C4 carbonyl group of U_1 and the H76 side chain, and between the C2 carbonyl group of U_3 and the R467 side chain. UUU in the *Mm*TLR7-Loxo-polyU complex adopts highly similar conformations (Figure S2C). Because U_2 was specifically recognized but U_1 and U_3 were loosely recognized, these findings indicate that diverse oligonucleotides can be recognized at the second site as long as they contain uridine.

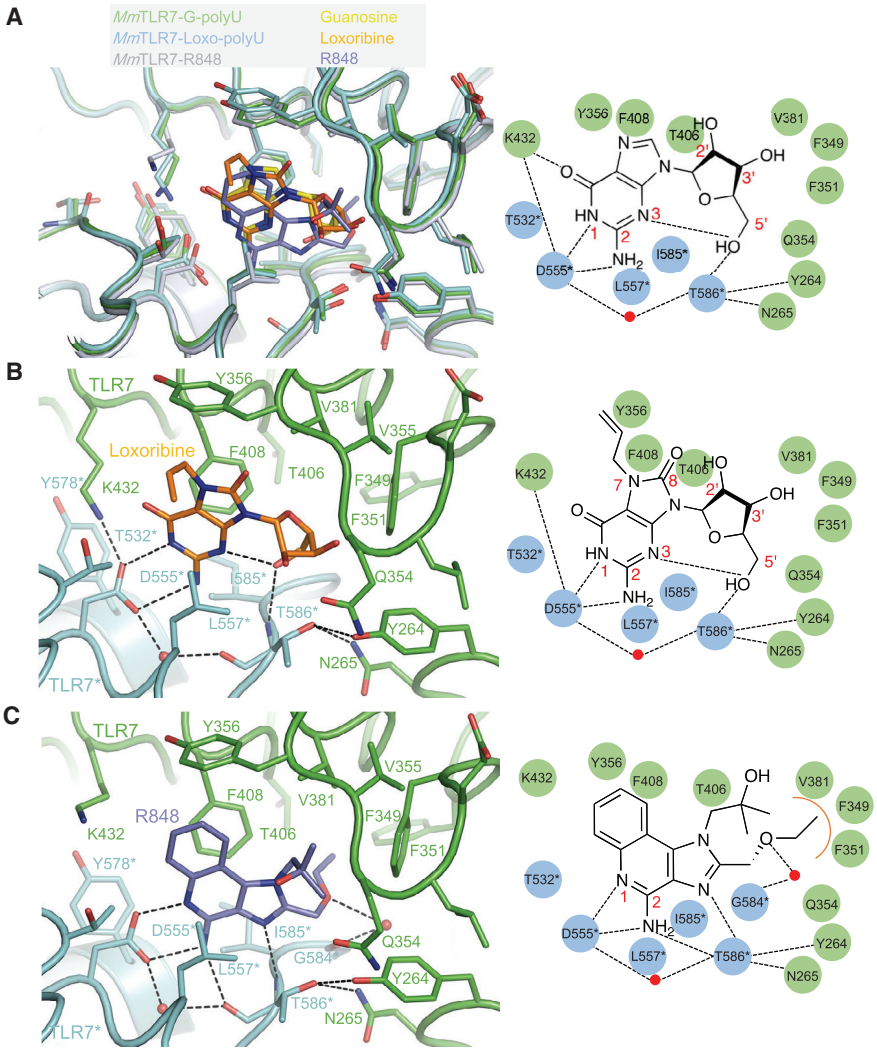

Figure 4. Recognition Mechanism of Guanosine, Loxoribine and R848 by TLR7 at the First Site

(A) Left, overlay of three first-site ligands, guanosine (yellow), loxoribine (orange), and R848 (light purple), in the structures of *Mm*TLR7-G-polyU (green), *Mm*TLR7-Loxo-polyU (cyan), and *Mm*TLR7-R848 (gray), respectively. Right, schematic representation of interactions between guanosine and TLR7 in the *Mm*TLR7-G-polyU structure. The red sphere indicates a water molecule. Hydrogen bonds are indicated by dashed lines.

(B) Left, magnified view of the first site of the *Mm*TLR7-Loxo-polyU structure. Right, schematic representation of interactions between loxoribine and TLR7.

(C) Left, magnified view of the first site of the *Mm*TLR7-R848 structure. Right, schematic representation of interactions between R848 and TLR7. The orange arc indicates hydrophobic interactions between the ethoxymethyl group of R848 and TLR7.

See also Figures S2B and S4D.

Both the First and Second Sites Are Essential for the ssRNA-Induced TLR7 Activation

To validate the functional importance of the first and second sites, we mutated the residues of these sites to alanine and then conducted nuclear factor kappa-light-chain-enhancer of activated B cells (NF-κB) dependent luciferase reporter assays; in these assays, we expressed human TLR7 in human embryonic kidney 293 cells stably expressing the SV40 large T antigen (HEK293T cells) and stimulated the cells with the chemical ligand R848 and phosphorothioated RNA9.2 s (RNA9.2sS), or co-stimulated the cells with guanosine and phosphorothioated polyU_19-mer (polyU_19merS) (Figure 5A). Mutations in the residues F408, D555, L557, and T586, all of which directly recognized first-site ligands, completely abolished the responsiveness of TLR7 to all types of stimulation, which indicated that the first site was essential for both chemical ligand- and ssRNA-induced TLR7 activation. In accordance with the structural observation that K432 participated in the recognition of guanosine but not R848 (Figures 4A and 4C), the K432A mutant lost its responsiveness to ssRNA ligands but not R848 (Figure 5A). In contrast to the first-site mutations, most of the second-site mutations of TLR7 (alanine substitutions at I74, H76, R97, L105, E156, Q181, Y184, and R473) reduced but did not abolish the ability of the receptors to respond to R848, but the mutations severely impaired the response of the receptors to the ssRNA ligands. These results suggested that the second site was essential only for the ssRNA-induced activation of TLR7.

The importance of the second site in ssRNA binding was further confirmed by performing gel-filtration chromatography analyses by using the recombinant mutant proteins (Figure 5B). In agreement with the results of the NF-κB reporter assay, the second-site mutants showed reduced binding to polyU_12-mer when compared with wild-type TLR7, as judged based on the ratios of the absorbance at 260 and 280 nm, but the ability of the mutants to dimerize in response to R848 was not affected (Figure 5B). The lower affinities of second-site mutations (R97A, C112S, R186A) for polyU_12-mer were also confirmed by isothermal titration calorimetry (ITC) analysis (Figure S5A). Mutation of R186, which interacts with the phosphate backbone, resulted in either retention or slight reduction in NF-κB activity though this mutant had lower ability to bind polyU_12-mer. This retained activity in NF-κB assay was possibly due to the ssRNA with phosphothioate backbones. In fact, the R186A mutant had almost the same affinity for phosphothioated polyU_12-mer as did wild-type TLR7 (Figure S5B).

Residues that were located inside the dimerization interface but were not directly involved in ligand recogntion were also of functional importance. Mutations of E583, L528, and R553 to alanine or arginine substantially abolished the ability of the receptors to respond to both R848 and ssRNA ligands (Figure S3D).

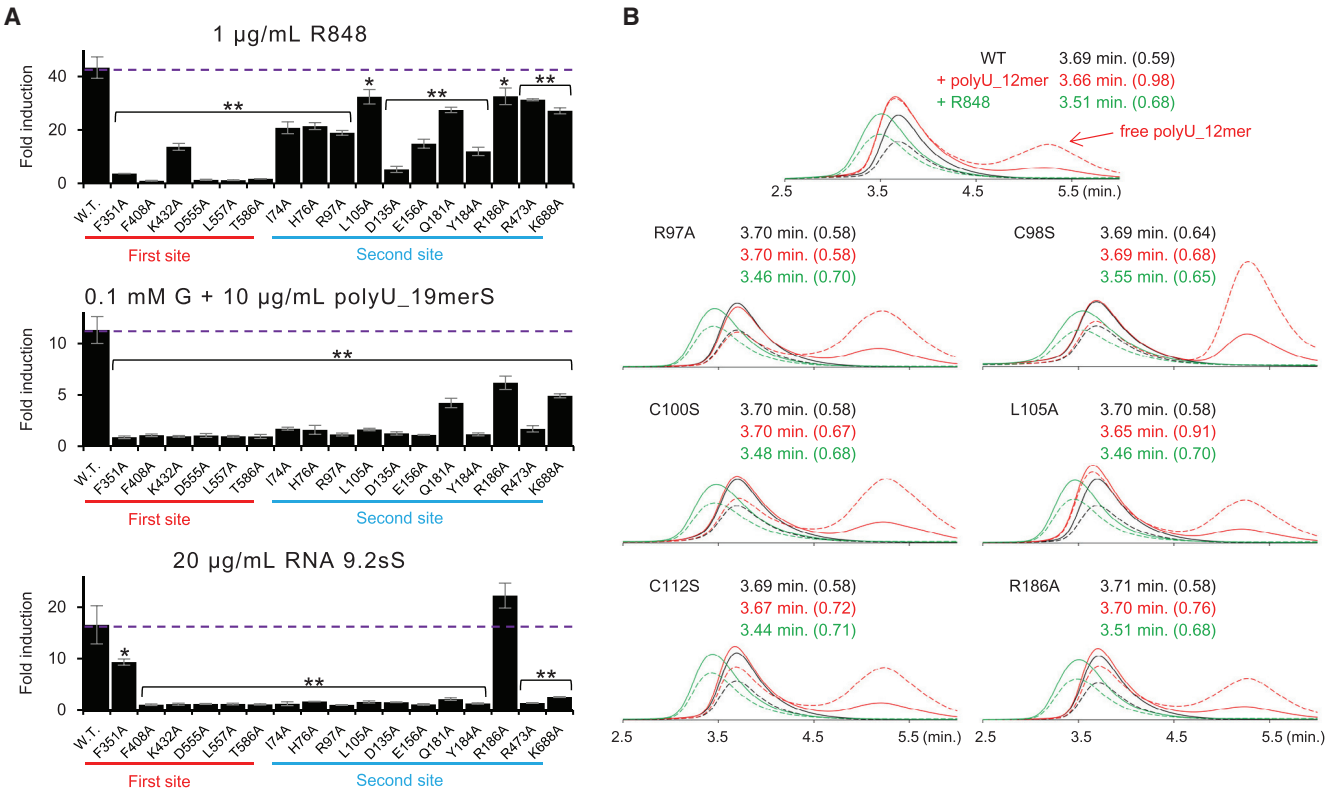

Figure 5. Both First and Second Sites Are Necessary for ssRNA-Induced TLR7 Activation

(A) NF-κB reporter activity measured for human TLR7 mutants expressed in HEK293T cells; cells were stimulated with 1 μg/mL R848 (top), 0.1 mM guanosine (G) + 10 μg/mL polyU_19merS (middle), and 20 μg/mL RNA9.2sS (bottom) (the suffix S in the ssRNA name indicates phosphorothioation). Data represent the mean fold induction of NF-κB activity (n = 3, +SD), calculated as the relative light units (RLU) of cells stimulated with the ligand divided by the RLU of non-stimulated cells. A paired t test was used to determine statistical significance between wild-type (WT) and each mutants. Double and single asterisks indicate $p < 0.01$ and $p < 0.05$ (t test), respectively. Dotted lines indicate a activity of WT. Data shown are representative of three independent experiments.

(B) Gel-filtration chromatography analysis of wild-type and mutant forms of *Mm*TLR7 without ligand (black) or with polyU_12-mer (red) or R848 (green). Absorbance values measured at 280 and 260 nm are indicated by solid and dotted lines, respectively. Elution times and the ratios of absorbance at 260 and 280 nm (in parenthesis) are shown.

See also Figures S3D and S6.

Our results showed that the first site was indespensible for TLR7 activation by all types of ligands, whereas the second site was only essential for the ssRNA-induced activation.

TLR7 Senses Guanosine and Shows Synergistic Activation by Oligonucleotides

TLR7 has been reported to function as a guanosine sensor based on the results of a cell-based assay (Shibata et al., 2015), and our structural work here revealed, at an atomic level, the mechanism by which guanosine was recognized by TLR7. To bolster these findings, we first performed ITC analysis (Table 2; Figure S6) to determine the binding affinity of TLR7 for various nucleosides (guanosine, adenosine, thymidine, cytidine, uridine, inosine, and xanthosine) and also chemical ligands (R848 and loxoribine). In accordance with the structural features, binding affinity could be determined only for guanosine among the nucleosides tested with a dissociation constant (K_d) value of 13.5 μM. As compared to guanosine, R848 and loxoribine bound to TLR7 more strongly (K_d = 0.49 and 5.6 μM, respectively) (Table 2A; Figure S6A).

Next, we examined the synergistic activation of TLR7 by either guanosine or chemical ligands and the oligonucleotides by performing ITC, gel-filtration chromatography, and sedimentation velocity analytical ultracentrifugation (SV-AUC) analyses. ITC analysis was used to measure the binding affinity of guanosine or chemical ligands (R848 and loxoribine) for TLR7 in the presence of polyU (Table 2B; Figure S6B). The affinities of guanosine, loxoribine, and R848 for TLR7 were markedly enhanced (to K_d = 0.93, 0.57, and 0.10 μM, respectively) in the presence of polyU_19-mer. Moreover, polyU_12-mer, polyU_9-mer, and polyU_6-mer enhanced the affinity for guanosine to similar extents, yielding K_d values of 1.2, 1.6, and 1.5 μM, respectively. In agreement with these findings, the results of gel-filtration analysis showed that guanosine and polyU_12-mer acted synergistically and caused TLR7 dimerization, and the results of SV-AUC analysis showed that the dimeric proportion was increased when guanosine and polyU were added together (Figures 1B and S7A–S7C).

As UUU bound at the second binding site was not directly involved in TLR7 dimerization (Figures S3A–S3C), we hypothesized that polyU did not directly induce the dimerization of TLR7. We performed SV-AUC analysis to examine the ability of polyU of various lengths to trigger TLR7 dimerization.

Table 2. Isothermal Titration Calorimetry Data

	Cell			Titrant					
	C_{TLR7} (μM)	RNA	C_{RNA} (μM)	Ligand	C_{ligand} (μM)	K_d (μM)	Δ*H* (kcal/M)	Δ*S* (cal/mol/deg)	*N*
A	100	-	-	Guanosine	1000	13.5	−10.8	−14.0	0.64
	100	-	-	Loxoribine	1000	5.6	−10.1	−9.7	0.85
	100	-	-	R848	1000	0.49	−4.1	15.1	0.71
	30	-	-	Uridine	1000	N.D			
	30	-	-	Adenosine	1000	N.D			
	30	-	-	Thymidine	1000	N.D			
	30	-	-	Cytidine	1000	N.D			
	30	-	-	Inosine	1000	N.D			
	30	-	-	Xanthosine	1000	N.D			
B	30	polyU_19-mer	30	Guanosine	250	0.93	−9.3	−3.5	0.57
	30	polyU_19-mer	30	Loxoribine	300	0.57	−7.6	3.1	0.71
	30	polyU_19-mer	30	R848	300	0.10	−2.4	23.6	0.53
	30	polyU_12-mer	30	Guanosine	300	1.2	−10.2	−7.2	0.69
	30	polyU_9-mer	30	Guanosine	300	1.6	−9.8	−6.5	0.60
	30	polyU_6-mer	30	Guanosine	300	1.5	−7.1	2.9	0.55
C	10	-	-	polyU_19-mer	100	0.37	−32.3	−78.8	0.42
	10	-	-	polyU_12-mer	100	0.08	−20.1	−34.8	0.65
	10	-	-	polyU_9-mer	100	0.09	−25.2	−52.3	0.49
	10	-	-	polyU_6-mer	100	0.22	−21.4	−41.2	0.50
	10	-	-	polyU_3-mer	100	N.D			
D	30	-	-	Guanosine	1000	7.6	−2.0	16.6	1.62
	30	UUU	30	Guanosine	1000	3.9	−6.9	1.7	0.94
	30	AAA	30	Guanosine	1000	9.2	−2.0	16.3	1.75
	30	GGG	30	Guanosine	1000	12.0	−2.4	14.3	1.27
	30	CCC	30	Guanosine	1000	10.2	−2.1	15.8	1.60
	30	UCU	30	Guanosine	1000	9.7	−2.4	15.0	1.46
	30	UGU	30	Guanosine	1000	9.8	−2.4	14.7	1.36

Each result was generated from a single titration. All data were collected using identical proteins purified at the same time. N.D stands for "not detected." See also Figure S6.

PolyU_6-mer and _9-mer alone did not induce the dimerization of TLR7 (Figures 1B and S7A), although their binding affinities for TLR7 were as high as those of polyU_12-mer and polyU_19-mer (Table 2C; Figure S6C). Conversely, the addition of guanosine effectively induced TLR7 dimerization (Figure S7B). To further characterize the dimerization of TLR7 in the presence of polyU together with/without guanosine by using SV-AUC, we analyzed the isotherms of weight-average sedimentation coefficients as a function of protein concentration. Concentration-dependent dimerization of TLR7 was observed, and the K_d values for the dimer formed with and without guanosine were estimated to be approximately 3 and 77 μM, respectively (Figure S7C). PolyU_19-mer and polyU_12-mer used alone also induced the dimerization of TLR7 (Figure S7A); however, we did not consider this to correspond to the activated form of the dimer because such long RNAs could concurrently bind to multiple TLR7 molecules.

Biochemical and biophysical studies here demonstrated that TLR7 exhibited preference for guanosine among nucleosides although its binding was weak. ssRNA alone did not directly induce the activation of TLR7 but enhanced the affinity of TLR7 for guanosine. TLR7 showed the synergistic actiivation by guanosine and ssRNA.

A Non-Terminal Uridine in RNA Is a Prerequisite for the Synergistic Effect on TLR7

To investigate whether TLR7 discriminated between ssRNA and ssDNA, we examined the binding of polydU by performing gel-filtration chromatography. Relative to polyU_12-mer, polydU_12-mer showed extremely weak binding to TLR7, as determined from the ratios of the absorbance at 260 and 280 nm (1.02 for polyU_12-mer versus 0.59 for polydU_12-mer), which demonstrated that TLR7 prefered ssRNA to ssDNA (Figure S7D). This agreed with the structural feature that the 2′-OH group of the U_2 ribose in UUU at the second site was recognized by Q181 and R473 (Figure 3D).

Next, we investigated the ssRNA sequence specificity of the second site. Our structural analysis had revealed that only the U_2 moiety of UUU was strictly recognized through uridine-specific interactions. To verify that the uridine was essential for the synergistic effect, we conducted ITC analysis by using trinucleotides (UUU, AAA, GGG, CCC, UCU, and UGU) (Table 2D;

Figure S6D), and found that among these trinucleotides, only UUU exhibited a synergistic effect on guanosine binding to TLR7. The K_d for guanosine was changed from 7.6 to 3.9 μM in the presence of UUU. We could not detect the direct binding of UUU to TLR7 in the ITC experiment, and RNA shortening reduced the synergistic effect to certain extent (Tables 2B–2D), but the synergism was still observed in the case of UUU, which indicated that UUU bound to TLR7. By contrast, none of the other trinucleotides tested—all of which lacked a uridine in the second position—affected any of the ITC parameters (K_d, ΔH, ΔS, and N values) measured for guanosine binding to TLR7, which indicated that these trinucleotides did not bind to TLR7. These results demonstrated that a uridine at a non-terminal position is indispensable for ssRNA binding to TLR7.

DISCUSSION

Here, we have reported the crystal structures of the activated forms of TLR7 complexed with agonistic ligands. Members of the TLR7 family are considered to remain inactive until Z-loop processing occurs in the endosomal compartment (Ewald et al., 2011; Ewald et al., 2008; Hipp et al., 2013; Ishii et al., 2014; Kanno et al., 2013; Ohto et al., 2015; Park et al., 2008; Sepulveda et al., 2009; Tanji et al., 2016). Previous work has demonstrated that the precise cleavage site of mouse TLR7 is after L460 or E461 (L460 or E461 in *Mm*TLR7) and that the generated N-terminal fragment remains associated with the C-terminal fragment through the C98-C475 disulfide bond that is crucial for TLR7 activation (Kanno et al., 2013). *Mm*TLR7 used in this study was artificially cleaved after the position 443 and the resultant N- and C-terminals were found to be cooperatively involved in ligand recognition, which suggested that the precise site of cleavage in TLR7 was not critical. The results of our structural and mutational analyses also demonstrated the importance of the unique disulfide bond in TLR7 between the N- and C-terminal fragments (C98–C475) for the formation of the second binding site and ssRNA recognition.This study has also revealed similarities and differences in the functional significance of the Z-loop among the receptors TLR7, TLR8, and TLR9. Although one of most critical functions of the Z-loop is to prevent receptor dimerization by sterically occluding the approaching dimerization partner, as recently demonstrated structurally in TLR8 (Tanji et al., 2016), the Z-loop of TLR7 also participated in the ssRNA recognition.

Our study has revealed that TLR7 specifically accommodated guanosine. In the case of the pyrimidine nucleosides cytidine, thymidine, and uridine, the recognition mode would be impaired due to their molecular size, whereas adenosine was not preferred because it lacks the 2-amino group, which, in guanosine, is specifically recognized by D555*. The similarities in the amino acids and the structure of the first site between TLR7 and TLR8 (43% identity, 72% similarity) explained why both can accommodate certain imidazoquinoline compounds such as R848 and gardiquimod. Conversely, TLR7 and TLR8 preferentially bind to guanosine and uridine nucleosides, respectively (Shibata et al., 2015; Tanji et al., 2015). Although the recognition modes used by these receptors are highly similar, the volume of their ligand-binding pocket and the electrostatic potentials at the pocket entrance (L557 in human TLR7, D545 in human TLR8) are distinct, and this might account for their divergent nucleoside specificity. Further studies will be required to address it.

TLR7 is activated by guanosine analogs such as deoxyguanosine, 8-hydroxydeoxyguanosine, 7-thia-8-oxoguanosine, and loxoribine (Lee et al., 2003; Shibata et al., 2015). We demonstrated that loxoribine bound to TLR7 in a similar manner as guanosine. Thus, the addition of the substituent at N7 and C8 of the guanine base could be tolerated, and the binding affinity of loxoribine was even slightly higher than that of guanosine. The ribose-specific 2′-OH group did not engage in any specific interaction, which can explain why 2′-deoxyguanosine exhibited similar affinity as guanosine (Shibata et al., 2015). As compared with guanosine, 8-hydroxydeoxyguanosine exhibited lower affinity, but induced a stronger cellular response (Shibata et al., 2015); however, a caveat to consider is that the biological response measured in a cellular assay is affected not only by ligand affinity but also by the transportation process and the metabolic stability of the ligand.

The sequence specificity of TLR7 activation has been widely studied, but no specific consensus sequences involved in activating TLR7 have thus far been identified conclusively (Diebold et al., 2004; Diebold et al., 2006; Heil et al., 2004; Hornung et al., 2005). We demonstrated that uridine was essential for ssRNA binding to the second site of TLR7. Furthermore, in terms of ssRNA length, we observed the synergistic effect when we used the 3-mer UUU. Therefore, by combining this finding with the structural observation that 3-mer RNA is specifically recognized, we concluded that ssRNAs longer than a 3-mer and containing a uridine base in non-terminal positions could potentially activate TLR7.

Guanosine alone cannot effectively activate TLR7 in cellular assays (Heil et al., 2004; Lee et al., 2003; Shibata et al., 2015), partly because the binding affinity of guanosine for TLR7 is lower than that of the chemical ligand R848. Therefore, the collaboration of the ssRNAs was indispensable here, as in the case of TLR8 (Tanji et al., 2015). The binding of guanosine to TLR7 was strengthened > 10-fold in the presence of polyU, and the resultant K_d, approximately 1.0 μM, was comparable to that of R848. Similar synergistic effects were also observed with loxoribine and R848. Considering that the Z-loop interacted with the loop regions of LRR2 and LRR5 in the dimerization interface, and with LRR8 and LRR11 of the first site, we speculated that the mechanism underlying the synergistic effect involved ssRNA-dependent stabilization of both the first and second sites, leading to a conformation that was more suitable for dimerization.

To summarize, our findings have uncovered a mechanism of TLR7 activation (Figure S7E): In the process of viral ssRNA recognition, TLR7 acts as a dual receptor for guanosine and uridine-containing ssRNAs, and ssRNA binding to the second site primes TLR7 for interaction with guanosine at the first site and subsequent dimerization. Conversely, chemical ligands are adequately potent to induce TLR7 dimerization by binding to the first site alone. The concept that TLR7 activation can be regulated by two distinct ligand-binding sites will facilitate not only further understanding of the functional role of TLR7, but also the development of therapeutic interventions.

EXPERIMENTAL PROCEDURES

Protein Expression, Purification, and Crystallization

The DNA encoding the extracellular domain of TLR7 from *Macaca mulatta* (*Mm*), followed by a thrombin-cleavage sequence (LVPRGS) and a protein A tag, was inserted into pMT/BiP/V5-His vector. To mimic the cleavage at the Z-loop, residues 440-445 were replaced by a thrombin-cleavage sequence. To prepare proteins with less glycosylation for crystallization, four Asn residues were mutated to Gln residues (N167Q, N389Q, N488Q and N799Q). *Drosophila* S2 cells were stably co-transfected with the TLR7 and pCoHygro vectors. Protein expression was induced by addition of 0.5 mM $CuSO_4$. For the expression of crystallization samples, 1.5 mg/L kifunensine (kif) was added into the culture medium. Proteins were purified by immunoglobulin G Separose from culture supernatant and was incubated overnight at 4°C with thrombin. Kif-untreated samples were then purified by Superdex 200 gel filtration chromatography in 10 mM Tris-HCl pH 7.5 and 0.15 M NaCl, and used for ITC, SV-AUC, and gel-filtration chromatography analyses. Kif-treated samples for crystallization were incubated overnight at 25°C with endo Hf for saccharide trimming and then purified by gel-filtration chromatography.

Crystallization were conducted with sitting-drop vapor-diffusion methods at 20°C. The droplets were made by mixing the equivolume (0.3–1.0 μL) of protein solution and reservoir solution. Detailed crystallization conditions were summarized in Table S1.

Data Collection and Structure Determination

Diffraction datasets were collected with a wavelength of 1.0000 Å on beamlines PF-AR NE3A (Ibaraki, Japan) and SPring-8 BL41XU (Hyogo, Japan) under cryogenic conditions at 100 K. Crystals were soaked into cryoprotectant solutions (Table S1) and were flash cooled in the cryostream or liquid nitrogen. The diffraction datasets were processed with the HKL2000 package (Otwinowski and Minor, 1997) or XDS (Kabsch, 2010). The initial phases for *Mm*TLR7-G-polyU were determined with the molecular replacement method by using the program MOLREP (Vagin and Teplyakov, 2010) with the coordinates of the human TLR8 structure (PDB ID: 3W3J). The model was further refined with stepwise cycles of manual model building using the COOT (Emsley and Cowtan, 2004) program and restrained refinement using REFMAC (Murshudov et al., 1997). The qualities of the final structures were validated with the PDB validation server (http://wwpdb-validation.wwpdb.org/). The statistics of the data collection and refinement are summarized in Table 1. The figures representing structures were prepared with PyMOL.

NF-κB-Dependent Luciferase Reporter Assay

HEK293T cells were cultured in DMEM with 10% FBS, 1X penicillin-streptomycin-glutamine and 50 μM 2-ME. HEK293T cells were seeded in collagen-coated 24-well plates at a density of 2×10^5 cells per well, and transiently transfected with wild-type or mutant human TLR7 cDNAs in pMX-puro-IRES-rat CD2 plasmid (200 ng), together with mouse Unc93B1 cDNA in pMX-puro plasmid (200 ng) and a pELAM1-luc reporter plasmid (1 ng), using PEI (Polyethylenimine "Max," MW 40,000). At 30 hr post-transfection, transfected cells, reseeded in collagen-coated flat 96 well plates at a density of 5×10^4 cells per well, were stimulated with indicated ligands for 6 hr and subjected to luciferase assay using the Luciferase Assay System (Promega). When cells were stimulated by RNA9.2sS alone, the ligand was complexed with 30 μL/mL DOTAP transfection reagent. The relative light unit of chemiluminescence was measured by GloMax Explorer (Promega).

Isothermal Titration Calorimetry

ITC experiments were carried out at 25°C in the buffer condition of 10 mM MES pH 5.5 and 150 mM NaCl by using a MicroCal iTC200 (GE Healthcare). The titration sequence included a single 0.4 μl injection followed by 18 injections, 2 μl each.

Liquid Chromatography-Mass Spectrometry Analysis of Dissolved Crystals

Crystals of *Mm*TLR7-G-polyU was washed three times with 4 M NaCl, 10 mM sodium HEPES, pH 7.0, and dissolved into 10 μl of 10 mM MES buffer pH 5.5 containing 50 mM NaCl. The detailed procedures of the LC-MS analysis were carried out as described previously (Taoka et al., 2009).

Sedimentation Velocity Analytical Ultracentrifugation

Samples for AUC were prepared so that the final salt concentrations were identical (147 mM NaCl, 8.3 mM MES, and 1.5 mM Tris) and pH was 5.5. SV–AUC experiments were conducted at 20°C in a ProteomeLab XL-I analytical ultracentrifuge (Beckman Coulter) at 42,000 rpm using absorbance optics.

Gel Filtration Chromatography Analysis of TLR7

The recombinant *Mm*TLR7 without the glycosylation mutations was subjected to gel-filtration chromatography using Superdex 200 Increase 5/150 GL column (GE Healthcare) in the presence of various ligands. Buffer used for the chromatography contained 10 mM MES pH 5.5 and 150 mM NaCl.

More detailed experimental procedures were provided in Supplemental Experimental Procedures.

ACCESSION NUMBERS

The coordinate and structure factor data of *Mm*TLR7-G-polyU, *Mm*TLR7-Loxo-polyU, and *Mm*TLR7-R848 have been deposited to the Protein Data Bank (PDB) under the PDB IDs 5GMF, 5GMG, and 5GMH, respectively.

SUPPLEMENTAL INFORMATION

Supplemental Information includes seven figures, one table, and Supplemental Experimental Procedures and can be found with this article online at http://dx.doi.org/10.1016/j.immuni.2016.09.011.

AUTHOR CONTRIBUTIONS

U.O. and H.T. performed initial trials of protein expression, purification, and crystallization. Z.Z. performed expression, purification, crystallization, and structure determination with assistance from U.O. Z.Z. performed SEC and ITC analyses. E.K. and S.U. performed AUC analyses. T. Shibata and K.M. performed cellular assays. M.T., Y.Y., and T.I. performed LC-MS experiment. Z.Z, U.O., and T. Shimizu wrote the paper with assistance from all other authors.

ACKNOWLEDGMENTS

We thank the beamline staff members at Photon Factory and SPring-8 for their assistance with data collection. This work was supported by a Grant-in-Aid from the Japanese Ministry of Education, Culture, Sports, Science, and Technology (U.O., T. Shibata, S.U., K.M., and T. Shimizu.); CREST, JST, (T. Shibata, T. Shimizu, T.I.); the Takeda Science Foundation (U.O. and T. Shimizu.); the Mochida Memorial Foundation for Medical and Pharmaceutical Research (U.O.); and the Daiichi Sankyo Foundation of Life Science (U.O.). The data presented in this manuscript are tabulated in and the Supplemental Information. The coordinates and structure-factor data have been deposited in the Protein Data Bank.

Received: May 23, 2016
Revised: June 13, 2016
Accepted: June 30, 2016
Published: October 11, 2016

REFERENCES

Aderem, A., and Ulevitch, R.J. (2000). Toll-like receptors in the induction of the innate immune response. Nature *406*, 782–787.

Alexopoulou, L., Holt, A.C., Medzhitov, R., and Flavell, R.A. (2001). Recognition of double-stranded RNA and activation of NF-kappaB by Toll-like receptor 3. Nature *413*, 732–738.

Bell, J.K., Mullen, G.E., Leifer, C.A., Mazzoni, A., Davies, D.R., and Segal, D.M. (2003). Leucine-rich repeats and pathogen recognition in Toll-like receptors. Trends Immunol. *24*, 528–533.

Diebold, S.S., Kaisho, T., Hemmi, H., Akira, S., and Reis e Sousa, C. (2004). Innate antiviral responses by means of TLR7-mediated recognition of single-stranded RNA. Science *303*, 1529–1531.

Diebold, S.S., Massacrier, C., Akira, S., Paturel, C., Morel, Y., and Reis e Sousa, C. (2006). Nucleic acid agonists for Toll-like receptor 7 are defined by the presence of uridine ribonucleotides. Eur. J. Immunol. *36*, 3256–3267.

Emsley, P., and Cowtan, K. (2004). Coot: model-building tools for molecular graphics. Acta Crystallogr. D Biol. Crystallogr. *60*, 2126–2132.

Ewald, S.E., Lee, B.L., Lau, L., Wickliffe, K.E., Shi, G.P., Chapman, H.A., and Barton, G.M. (2008). The ectodomain of Toll-like receptor 9 is cleaved to generate a functional receptor. Nature *456*, 658–662.

Ewald, S.E., Engel, A., Lee, J., Wang, M., Bogyo, M., and Barton, G.M. (2011). Nucleic acid recognition by Toll-like receptors is coupled to stepwise processing by cathepsins and asparagine endopeptidase. J. Exp. Med. *208*, 643–651.

Heil, F., Ahmad-Nejad, P., Hemmi, H., Hochrein, H., Ampenberger, F., Gellert, T., Dietrich, H., Lipford, G., Takeda, K., Akira, S., et al. (2003). The Toll-like receptor 7 (TLR7)-specific stimulus loxoribine uncovers a strong relationship within the TLR7, 8 and 9 subfamily. Eur. J. Immunol. *33*, 2987–2997.

Heil, F., Hemmi, H., Hochrein, H., Ampenberger, F., Kirschning, C., Akira, S., Lipford, G., Wagner, H., and Bauer, S. (2004). Species-specific recognition of single-stranded RNA via toll-like receptor 7 and 8. Science *303*, 1526–1529.

Hemmi, H., Takeuchi, O., Kawai, T., Kaisho, T., Sato, S., Sanjo, H., Matsumoto, M., Hoshino, K., Wagner, H., Takeda, K., and Akira, S. (2000). A Toll-like receptor recognizes bacterial DNA. Nature *408*, 740–745.

Hemmi, H., Kaisho, T., Takeuchi, O., Sato, S., Sanjo, H., Hoshino, K., Horiuchi, T., Tomizawa, H., Takeda, K., and Akira, S. (2002). Small anti-viral compounds activate immune cells via the TLR7 MyD88-dependent signaling pathway. Nat. Immunol. *3*, 196–200.

Hipp, M.M., Shepherd, D., Gileadi, U., Aichinger, M.C., Kessler, B.M., Edelmann, M.J., Essalmani, R., Seidah, N.G., Reis e Sousa, C., and Cerundolo, V. (2013). Processing of human toll-like receptor 7 by furin-like proprotein convertases is required for its accumulation and activity in endosomes. Immunity *39*, 711–721.

Hornung, V., Guenthner-Biller, M., Bourquin, C., Ablasser, A., Schlee, M., Uematsu, S., Noronha, A., Manoharan, M., Akira, S., de Fougerolles, A., et al. (2005). Sequence-specific potent induction of IFN-alpha by short interfering RNA in plasmacytoid dendritic cells through TLR7. Nat. Med. *11*, 263–270.

Hoshino, K., Takeuchi, O., Kawai, T., Sanjo, H., Ogawa, T., Takeda, Y., Takeda, K., and Akira, S. (1999). Cutting edge: Toll-like receptor 4 (TLR4)-deficient mice are hyporesponsive to lipopolysaccharide: evidence for TLR4 as the Lps gene product. J. Immunol. *162*, 3749–3752.

Ishii, N., Funami, K., Tatematsu, M., Seya, T., and Matsumoto, M. (2014). Endosomal Localization of TLR8 Confers Distinctive Proteolytic Processing on Human Myeloid Cells. J Immunol. *193*, 5118–5128.

Janeway, C.A., Jr., and Medzhitov, R. (2002). Innate immune recognition. Annu. Rev. Immunol. *20*, 197–216.

Jurk, M., Heil, F., Vollmer, J., Schetter, C., Krieg, A.M., Wagner, H., Lipford, G., and Bauer, S. (2002). Human TLR7 or TLR8 independently confer responsiveness to the antiviral compound R-848. Nat. Immunol. *3*, 499.

Kabsch, W. (2010). Xds. Acta Crystallogr. D Biol. Crystallogr. *66*, 125–132.

Kanno, A., Yamamoto, C., Onji, M., Fukui, R., Saitoh, S., Motoi, Y., Shibata, T., Matsumoto, F., Muta, T., and Miyake, K. (2013). Essential role for Toll-like receptor 7 (TLR7)-unique cysteines in an intramolecular disulfide bond, proteolytic cleavage and RNA sensing. Int. Immunol. *25*, 413–422.

Lee, J., Chuang, T.H., Redecke, V., She, L., Pitha, P.M., Carson, D.A., Raz, E., and Cottam, H.B. (2003). Molecular basis for the immunostimulatory activity of guanine nucleoside analogs: activation of Toll-like receptor 7. Proc. Natl. Acad. Sci. USA *100*, 6646–6651.

Lehmann, S.M., Krüger, C., Park, B., Derkow, K., Rosenberger, K., Baumgart, J., Trimbuch, T., Eom, G., Hinz, M., Kaul, D., et al. (2012). An unconventional role for miRNA: let-7 activates Toll-like receptor 7 and causes neurodegeneration. Nat. Neurosci. *15*, 827–835.

Liu, L., Botos, I., Wang, Y., Leonard, J.N., Shiloach, J., Segal, D.M., and Davies, D.R. (2008). Structural basis of toll-like receptor 3 signaling with double-stranded RNA. Science *320*, 379–381.

Matsushima, N., Tanaka, T., Enkhbayar, P., Mikami, T., Taga, M., Yamada, K., and Kuroki, Y. (2007). Comparative sequence analysis of leucine-rich repeats (LRRs) within vertebrate toll-like receptors. BMC Genomics *8*, 124.

Murshudov, G.N., Vagin, A.A., and Dodson, E.J. (1997). Refinement of macromolecular structures by the maximum-likelihood method. Acta Crystallogr. D Biol. Crystallogr. *53*, 240–255.

Nagai, Y., Akashi, S., Nagafuku, M., Ogata, M., Iwakura, Y., Akira, S., Kitamura, T., Kosugi, A., Kimoto, M., and Miyake, K. (2002). Essential role of MD-2 in LPS responsiveness and TLR4 distribution. Nat. Immunol. *3*, 667–672.

Ohto, U., Fukase, K., Miyake, K., and Shimizu, T. (2012). Structural basis of species-specific endotoxin sensing by innate immune receptor TLR4/MD-2. Proc. Natl. Acad. Sci. USA *109*, 7421–7426.

Ohto, U., Shibata, T., Tanji, H., Ishida, H., Krayukhina, E., Uchiyama, S., Miyake, K., and Shimizu, T. (2015). Structural basis of CpG and inhibitory DNA recognition by Toll-like receptor 9. Nature *520*, 702–705.

Oldenburg, M., Krüger, A., Ferstl, R., Kaufmann, A., Nees, G., Sigmund, A., Bathke, B., Lauterbach, H., Suter, M., Dreher, S., et al. (2012). TLR13 recognizes bacterial 23S rRNA devoid of erythromycin resistance-forming modification. Science *337*, 1111–1115.

Otwinowski, Z., and Minor, W. (1997). Processing of X-ray diffraction data collected in oscillation mode. Methods Enzymol. *276*, 307–326.

Park, B., Brinkmann, M.M., Spooner, E., Lee, C.C., Kim, Y.M., and Ploegh, H.L. (2008). Proteolytic cleavage in an endolysosomal compartment is required for activation of Toll-like receptor 9. Nat. Immunol. *9*, 1407–1414.

Park, B.S., Song, D.H., Kim, H.M., Choi, B.S., Lee, H., and Lee, J.O. (2009). The structural basis of lipopolysaccharide recognition by the TLR4-MD-2 complex. Nature *458*, 1191–1195.

Poltorak, A., He, X., Smirnova, I., Liu, M.Y., Van Huffel, C., Du, X., Birdwell, D., Alejos, E., Silva, M., Galanos, C., et al. (1998). Defective LPS signaling in C3H/HeJ and C57BL/10ScCr mice: mutations in Tlr4 gene. Science *282*, 2085–2088.

Santiago-Raber, M.L., Baudino, L., and Izui, S. (2009). Emerging roles of TLR7 and TLR9 in murine SLE. J. Autoimmun. *33*, 231–238.

Savarese, E., Chae, O.W., Trowitzsch, S., Weber, G., Kastner, B., Akira, S., Wagner, H., Schmid, R.M., Bauer, S., and Krug, A. (2006). U1 small nuclear ribonucleoprotein immune complexes induce type I interferon in plasmacytoid dendritic cells through TLR7. Blood *107*, 3229–3234.

Sepulveda, F.E., Maschalidi, S., Colisson, R., Heslop, L., Ghirelli, C., Sakka, E., Lennon-Duménil, A.M., Amigorena, S., Cabanie, L., and Manoury, B. (2009). Critical role for asparagine endopeptidase in endocytic Toll-like receptor signaling in dendritic cells. Immunity *31*, 737–748.

Shibata, T., Ohto, U., Nomura, S., Kibata, K., Motoi, Y., Zhang, Y., Murakami, Y., Fukui, R., Ishimoto, T., Sano, S., et al. (2015). Guanosine and its modified derivatives are endogenous ligands for TLR7. Int Immunol.

Song, D.H., and Lee, J.O. (2012). Sensing of microbial molecular patterns by Toll-like receptors. Immunol. Rev. *250*, 216–229.

Song, W., Wang, J., Han, Z., Zhang, Y., Zhang, H., Wang, W., Chang, J., Xia, B., Fan, S., Zhang, D., et al. (2015). Structural basis for specific recognition of single-stranded RNA by Toll-like receptor 13. Nat. Struct. Mol. Biol. *22*, 782–787.

Takahashi, K., Asabe, S., Wieland, S., Garaigorta, U., Gastaminza, P., Isogawa, M., and Chisari, F.V. (2010). Plasmacytoid dendritic cells sense hepatitis C virus-infected cells, produce interferon, and inhibit infection. Proc. Natl. Acad. Sci. USA *107*, 7431–7436.

Takeuchi, O., and Akira, S. (2010). Pattern recognition receptors and inflammation. Cell *140*, 805–820.

Tanji, H., Ohto, U., Shibata, T., Miyake, K., and Shimizu, T. (2013). Structural reorganization of the Toll-like receptor 8 dimer induced by agonistic ligands. Science *339*, 1426–1429.

Tanji, H., Ohto, U., Shibata, T., Taoka, M., Yamauchi, Y., Isobe, T., Miyake, K., and Shimizu, T. (2015). Toll-like receptor 8 senses degradation products of single-stranded RNA. Nat. Struct. Mol. Biol. *22*, 109–115.

Tanji, H., Ohto, U., Motoi, Y., Shibata, T., Miyake, K., and Shimizu, T. (2016). Autoinhibition and relief mechanism by the proteolytic processing of Toll-like receptor 8. Proc. Natl. Acad. Sci. USA *113*, 3012–3017.

Taoka, M., Yamauchi, Y., Nobe, Y., Masaki, S., Nakayama, H., Ishikawa, H., Takahashi, N., and Isobe, T. (2009). An analytical platform for mass spectrometry-based identification and chemical analysis of RNA in ribonucleoprotein complexes. Nucleic Acids Res. *37*, e140.

Vagin, A., and Teplyakov, A. (2010). Molecular replacement with MOLREP. Acta Crystallogr. D Biol. Crystallogr. *66*, 22–25.

Wang, J.P., Bowen, G.N., Padden, C., Cerny, A., Finberg, R.W., Newburger, P.E., and Kurt-Jones, E.A. (2008). Toll-like receptor-mediated activation of neutrophils by influenza A virus. Blood *112*, 2028–2034.